Available online at www.sciencedirect.com

ScienceDirect

journal homepage: www.elsevier.com/locate/he

One-step synthesis of AuPd alloy nanoparticles on graphene as a stable catalyst for ethanol electro-oxidation

Changhai Liu [a,b], *Xinlei Cai* [b], *Jianshe Wang* [c], *Jie Liu* [b], *Adam Riese* [d], *Zhidong Chen* [a], *Xueliang Sun* [d,**], *Sui-Dong Wang* [b,*]

[a] *School of Materials Science & Engineering, Jiangsu Collaborative Innovation Center of Photovoltaic Science and Engineering, Changzhou University, Changzhou, Jiangsu 213164, PR China*

[b] *Soochow University-Western University Joint Centre for Synchrotron Radiation Research, Institute of Functional Nano & Soft Materials (FUNSOM), Soochow University, Suzhou, Jiangsu 215123, PR China*

[c] *School of Chemical Engineering and Energy, Zhengzhou University, Zhengzhou 450000, PR China*

[d] *Department of Mechanical and Materials Engineering, Western University, ON N6A 5B9, Canada*

ARTICLE INFO

Article history:
Received 23 February 2016
Received in revised form
30 April 2016
Accepted 21 May 2016
Available online 8 June 2016

Keywords:
AuPd nanoparticles
Ionic liquids
Graphene
Ethanol electro-oxidation
Sputter deposition

ABSTRACT

Room-temperature-ionic-liquid-assisted sputtering with an alloy target is utilized to synthesize the graphene-supported AuPd alloy nanoparticles, whose Au-to-Pd ratio can be well controlled. The preparation process is one-step, free of additives and stabilizers. For direct electro-oxidation of ethanol in alkaline media, the supported AuPd alloy nanoparticles show much higher catalytic activity compared with a commercial Pd/C catalyst and the monometallic counterpart. The optimal Au-to-Pd ratio is 1:3, and the nanocatalyst of AuPd (1:3) possesses high stability and durability. After 500 cyclic voltammetry test cycles, the anodic peak current density for ethanol electro-oxidation still remains about 91% of the initial one. Furthermore, by quantitatively analyzing the relative reactivity retention, the alloy nanoparticle catalysts with graphene as the support show much higher anti-poisoning performance than the corresponding monometallic catalysts with active C as the support.

Introduction

Direct alcohol fuel cells (DAFCs), a type of alkaline fuel cells (AFC), are one of most promising energy conversion technologies that has attracted much attention in the recent decades [1–3]. The direct oxidation of methanol in fuel cells has been extensively investigated, though there are still some critical issues to be addressed, such as toxicity, environmental problems in relation to the miscibility of methanol to water [1]. Ethanol, which is the major renewable biofuel from fermentation of biomass and can be produced in large quantities from agricultural products, offers an attractive alternative as a fuel in low-temperature fuel cells. Direct ethanol fuel

* *Corresponding author*. Fax: +86 512 65883521.
** *Corresponding author*. Fax: +86 512 65883521.
E-mail addresses: xsun@eng.uwo.ca (X. Sun), wangsd@suda.edu.cn (S.-D. Wang).
http://dx.doi.org/10.1016/j.ijhydene.2016.05.194

cells (DEFCs) show high energy-conversion efficiency, low operation temperature and simple handling of the fuel, as well as convenience to use [4–6]. Based on the foregoing works, the selective of ethanol to CO_2 is relatively low, and the ethanol oxidation in alkaline media follows mechanisms below:

$$CH_3CH_2OH + 3OH^- \leftrightarrow CH_3CO_{ads} + 3H_2O \quad (1)$$

$$OH^- \leftrightarrow OH_{ads} + e \quad (2)$$

$$CH_3CO_{ads} + OH_{ads} \rightarrow CH_3COOH \quad (3)$$

$$CH_3COOH + OH^- \rightarrow CH_3COO^- + H_2O \quad (4)$$

According to Eqs. (1)–(4), the rate-determining step in the ethanol oxidation reaction is Eq. (3) [4,6]. In addition, the catalytic activity of catalysts strongly depends on the pH value of electrolytes, and it is much stronger in alkaline media than in acidic ones. The reason of improved kinetics in alkaline media is that continued dehydrogenation of ethanol cannot readily proceed in acidic media due to the lack of OH species, which can instantly remove hydrogen [7,8]. Meanwhile, the stability, which is related to the structure, morphology and composition of catalysts, is an important factor as well for practical applications of DAFCs.

As we know, Pt-based and Pd-based alloys are widely used as catalysts in DAFCs due to their high catalytic performance [9–14]. However, high cost of Pt is a serious drawback for the commercialization of Pt-based fuel cell technology. In addition, another critical issue for Pt catalyst is less stability, showing up as attenuation fast of catalytic activity in current density-time (i-t) curve, due to the catalyst poisoning arising from the intermediate product [12,15]. Therefore, the development of Pt-free catalysts for fuel cells has been a hot topic in new energy investigations. It is noteworthy that naturally abundant Pd often shows higher catalytic activity than Pt in an alkaline electrolyte for electrocatalytic oxidation of ethanol [16]. Furthermore, forming Pd-based bimetallic catalysts, such as PdNi [17], PdCo [18,19], PdAg [20] and PdCu [21] alloys, can further enhance the catalytic activity and stability of Pd catalysts. In particular, AuPd bimetallic nanoparticles (NPs) have been demonstrated to possess enhanced catalytic activity for ethanol oxidation [22–24]. The improvement upon the addition of Au is attributed to the synergistic effect between two elements, such as ligand effect and ensemble effect [25–27]. The ligand effect refers to the electronic interactions between two components, and the ensemble effect is related to surface atomic arrangements and dilution. Both the effects are associated with the chemical composition and geometric shape of catalysts, and thus it is of great significance to effectively control their compositional ratio and morphology [27]. Moreover, an alternative approach can also be adopted to improve the activity and anti-poisoning performances of catalysts, normally called employing suitable supports.

Graphene is a one-atom-thick two-dimensional sheets of graphite with p-electrons fully delocalized on the graphite plane with a number of unusual properties, such as high thermal conductivity and mechanical stiffness, extraordinary electronic transport properties, and high specific surface area, to stabilize nanocatalysts such as metal NPs [28–31]. Because catalysis is a surface effect, catalysts often need to have a surface area as high as possible. The graphene-supported nanocatalysts can offer not only a high surface area but also a conductive surface, which is beneficial for electron transport in many catalytic processes. It has been demonstrated in the Pt-based and Pd-based NPs catalysts grown on graphene for electrocatalytic reactions [10,11,15]. Recently, Wang et al. proved that the metallic NPs supported on the surface of graphene show superior anti-poisoning performance for formate oxidation [32]. Therefore, it is necessary to combine the metallic NPs catalysts with graphene support toward the ethanol oxidation for high activity and superior anti-poisoning performance.

Recently, we developed an alternative approach to prepare graphene-supported AuPd alloy NPs by successively sputtering Au and Pd onto room temperature ionic liquids (RTILs), e.g. 1-butyl-3-methylimidazolium tetrafluoroborate [BMIm][BF_4] [33–36]. It is a universal and environmental-friendly method totally free of such as reducing and stabilizing agents. On the basis of the foregoing research, we extend this means to prepare AuPd alloy NPs on graphene straightforwardly from alloy targets with different Au-to-Pd ratios. The catalytic activities of graphene-supported AuPd alloy NPs show a strong dependence on the Au-to-Pd ratios, suggesting occurrence of the synergistic effects. Moreover, the nanocatalyst with an optimal composition of AuPd (1:3) exhibits much superior catalytic activity and stability for ethanol electro-oxidation.

Materials and methods

Materials

All chemicals used in this study were in analytical grade. Ethanol and KOH were purchased from Alfa Aesar and used as received. Graphene powder was purchased from Nanjing XFNANO Materials Tech, which is prepared by the thermal exfoliation reduction and hydrogen reduction. [BMIm][BF_4] (purity > 99%) was purchased from Shanghai Cheng-Jie Chemical and purified in vacuum for 24 h before using. Double-distilled water was used for the preparation of standard solution.

Preparation of graphene-supported metal NPs

As reported in our previous articles [33–35], the Au, Pd and AuPd alloy NPs were prepared via a RTIL-assisted sputtering deposition process. We replace the monometallic targets by AuPd alloying targets with different Au-to-Pd ratio to achieve uniform component ratios in the sputtered nanostructures. First, 10 mg graphene powder was fully dispersed into 1.5 ml [BMIm][BF_4] with ultrasonication for 10 min. Then, the black graphene-RTIL suspension was dropped into a clean stainless steel pot, and the metal of interest was sputtered onto the graphene-RTIL suspension at room temperature for 600 s in a desktop direct-current sputtering system (Quorum Technologies, equipped with a thickness monitor which is calibrated by a surface profiler). Eventually, the alloy NPs and monometallic NPs were separated from [BMIm][BF_4] with high-speed centrifugation and decantation, followed by washing

in an ultrasonic bath of acetone. This cleaning process was repeated several times to completely remove residual [BMIm][BF_4] from the graphene supported NPs hybrids (in dry powder form).

Characterization of graphene-supported metal NPs

The microscopic structures of the graphene-supported AuPd alloy NPs were characterized with high-resolution transmission electron microscopy (HRTEM, FEI Quanta FRG 200F, operating at 200 kV) and high-angle annular dark-field scanning TEM (HAADF-STEM). The crystalline structures of graphene-supported AuPd alloy NPs were characterized with X-ray diffraction (XRD, PANalytical Empyrean). The electronic structures of graphene-supported AuPd alloy NPs were characterized with X-ray photoemission spectroscopy (XPS, Kratos Axis Ultra DLD, monochromatic Al $K\alpha$) in ultrahigh vacuum. The inductive coupled plasma-atomic emission spectroscopy (ICP-AES) measurements were conducted with Varian Vista MPX, and the samples were digested in concentrated HNO_3 and then diluted to desired concentrations.

Electrochemical measurements

The electrochemical activities of the graphene-supported AuPd alloy NPs and commercial Pd/C (20 wt%; Sigma) catalysts were characterized by cyclic voltammetry (CV) and chronoamperometry (CA) techniques. The measurements were performed with a three-electrode cell in a CHI660E electrochemical workstation at ambient temperature. Typically, the catalyst dispersion was prepared by mixing 5 mg of catalysts in 2 ml of solution containing 2 ml of ethanol and 20 μL of 5 wt% Nafion solution followed by ultrasonication for 30 min. Glassy carbon (GC) electrode (3 mm in diameter) served as the substrate for the catalysts. Prior to use, the GC electrode was polished using aqueous alumina suspension, and then 10 μL aliquots of catalysts suspension was pipetted with a micropipettor onto the GC surface. An Ag/AgCl electrode and a Pt wire were used as the reference electrode and the counter electrode, respectively. The electrochemistry tests were carried out in an aqueous solution containing 1 mol/L potassium hydroxide (KOH) and 1 mol/L ethanol (C_2H_5OH), sweeping from −0.8 to 0.2 V at a scan rate of 50 mV/s. All potentials herein are relative to Ag/AgCl electrode, and all the electrochemical measurements are conducted at 25 °C in a N_2-saturated solution.

Results and discussion

As illustrated in Fig. 1, the microscopic structures of the graphene-supported Pd NPs and Au NPs are characterized with TEM and HRTEM. The supported Pd NPs shown in Fig. 1a and b have uniform size, around 2.54 nm. An identical interplanar spacing of 0.23 nm is present in the HRTEM image, indicating the crystallinity of the (111) lattice plane for face-

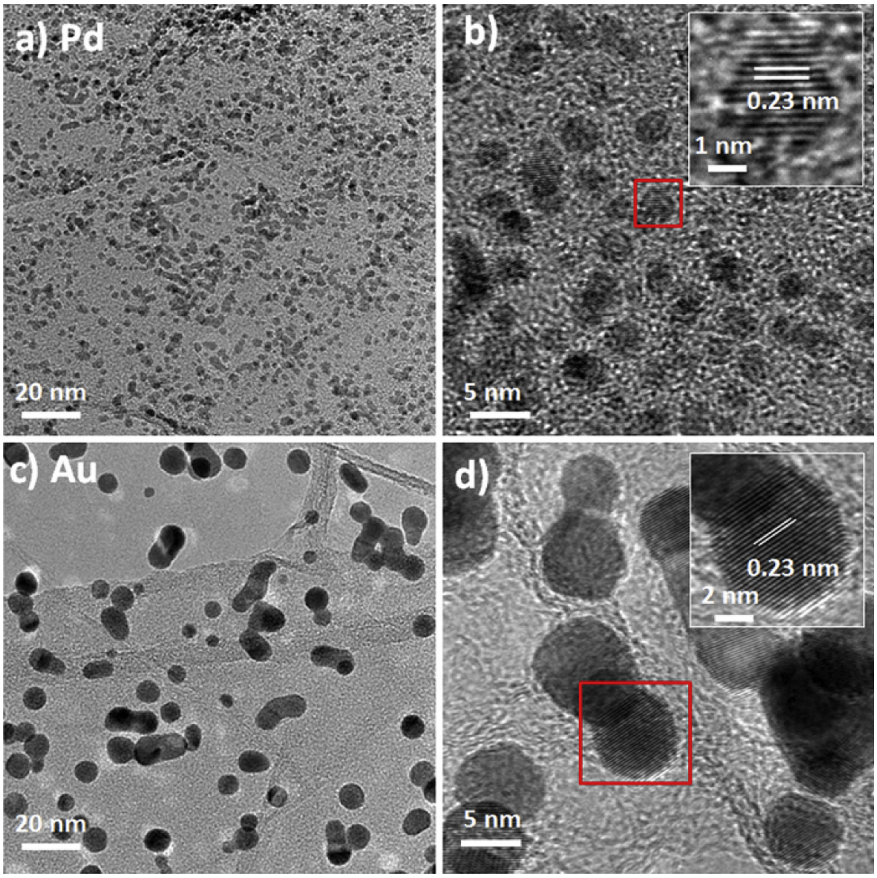

Fig. 1 – TEM and HRTEM images of (a) and (b): graphene-supported Pd NPs: (c) and (d): graphene-supported Au NPs.

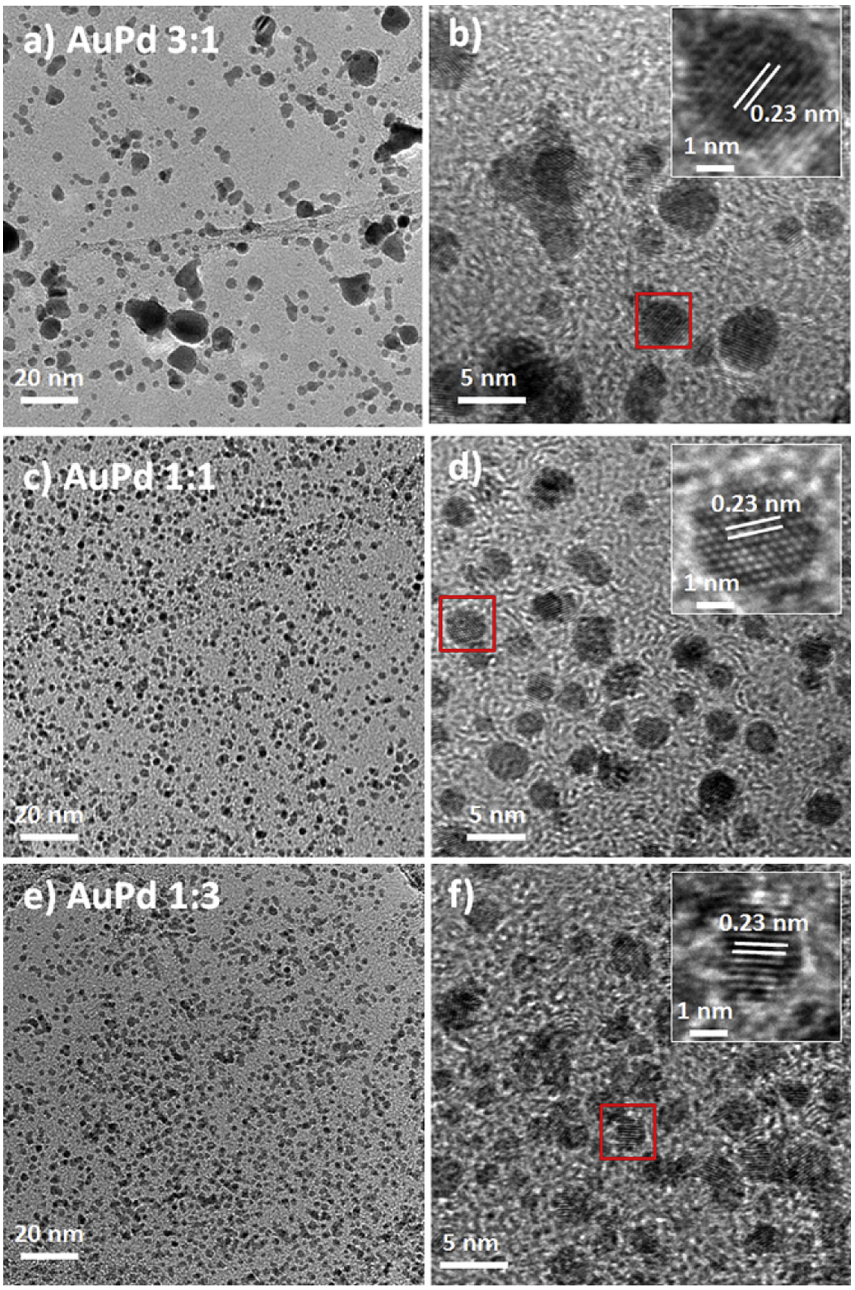

Fig. 2 – TEM and HRTEM images of graphene-supported AuPd alloy NPs with different Au-to-Pd ratios: (a) and (b) for 3:1; (c) and (d) for 1:1; and (e) and (f) for 1:3.

centered cubic (fcc) Pd. As for the supported Au NPs shown in Fig. 1c and d, the average size of Au NPs, up to 6.68 nm, is much larger than that of Pd NPs. The interplanar spacing of 0.23 nm corresponds to the (111) lattice plane of fcc Au [22,24]. The morphology of the Au and Pd NPs is quite different under the same preparation conditions, which may be associated with the extent of the interaction between RTILs and different kinds of metal NPs [33,37,38].

The TEM and HRTEM images of the graphene-supported AuPd alloy NPs with different Au-to-Pd ratios are shown in Fig. 2. Three AuPd alloy targets for the sputtering, with Au-to-Pd mole ratios of 3:1, 1:1 and 1:3, are selected for the sputtering. For AuPd (3:1) shown in Fig. 2a and b, the size distribution of NPs is not uniform, where the average diameter is about 4.51 nm. On the other hand, for AuPd (1:1), depicted in Fig. 2c and d, the size distribution of AuPd NPs becomes more uniform and narrow. In this case, the average diameter is 2.55 nm, which is much smaller than that of AuPd (3:1). With an increase of Pd content to AuPd (1:3), the average diameter of AuPd NPs is further reduced to 2.10 nm, as shown in Fig. 2e and f. All the samples show a same lattice spacing of 0.23 nm, which is similar to the monometallic NPs shown in Fig. 1.

To probe the microscopic structure for AuPd NPs, HADDF-STEM is utilized to study the elemental spatial distribution.

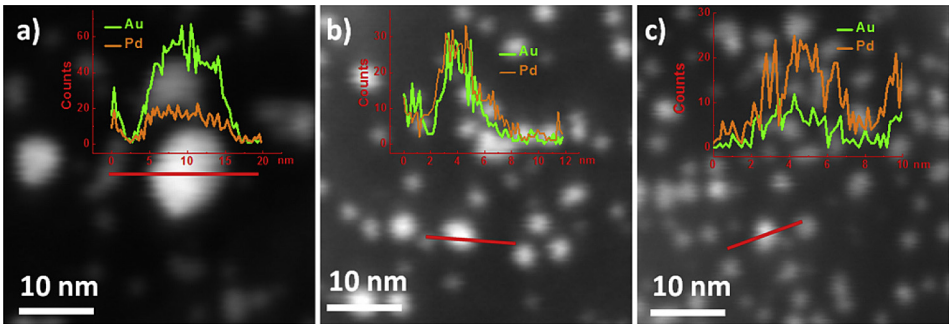

Fig. 3 – HAADF-STEM images and crossline profiles of elemental composition (based on EDS data) for graphene-supported AuPd alloy NPs with different Au-to-Pd ratios: (a) for 3:1; (b) for 1:1; and (c) for 1:3.

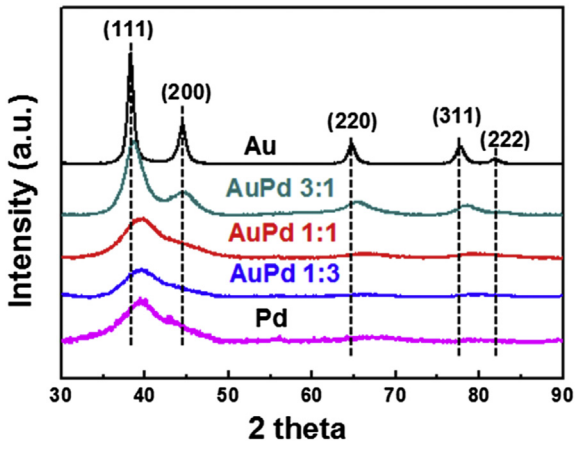

Fig. 4 – XRD patterns of graphene-supported AuPd (3:1), AuPd (1:1) and AuPd (1:3) alloy NPs, and of Au and Pd monometallic NPs as references.

The crossline profiles of the elemental composition for AuPd NPs with different Au-to-Pd ratio are shown in Fig. 3a, b and c, corresponding to AuPd (3:1), AuPd (1:1) and AuPd (1:3), respectively. The green and orange curves represent Au and Pd, respectively. There is a coexistence of both metal species in the NPs, indicating that the occurrence of local alloying. Considering that the preparation process is one-step sputtering deposition from the AuPd alloy targets, the formation of AuPd alloy NPs on graphene is reasonable. Furthermore, the energy dispersive spectroscopy (EDS) analysis shown in the insets in Fig. 3 suggests that the Au-to-Pd atomic ratios are close to the corresponding nominal composition predetermined in the alloy targets. The real percentages of Au and Pd are evaluated with ICP-AES. For AuPd (1:3), AuPd (1:1) and AuPd (3:1), the Au-to-Pd atomic ratios derived from ICP-AES are about 24:76, 44:56 and 77:23, respectively, which are highly consistent with those in the alloy targets. Therefore, it is easy and controllable to prepare AuPd alloy NPs with a precise Au-to-Pd ratio by employing the present RTILs-assisted sputtering method.

The XRD patterns of the metal NPs are shown in Fig. 4, where the crystalline features of Au (111), (200), (220), (311) and (222) are clearly present. However, the diffraction peaks of Pd are weak with a broad full-width at half-maximum (FWHM), owing to tiny size of Pd NPs. In the case of AuPd (3:1), all the diffraction peaks are shifted upward slightly compared to Au NPs. Meanwhile, peak FWHM for AuPd (3:1) are broadened as

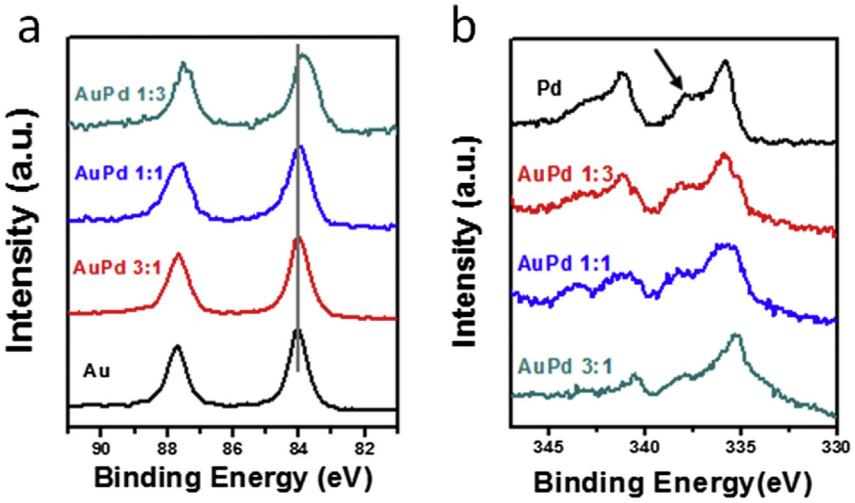

Fig. 5 – (a) XPS Au 4f spectra and (b) Pd 3d spectra for graphene-supported AuPd (3:1), AuPd (1:1) and AuPd (1:3) alloy NPs, and of Au and Pd monometallic NPs as references, respectively.

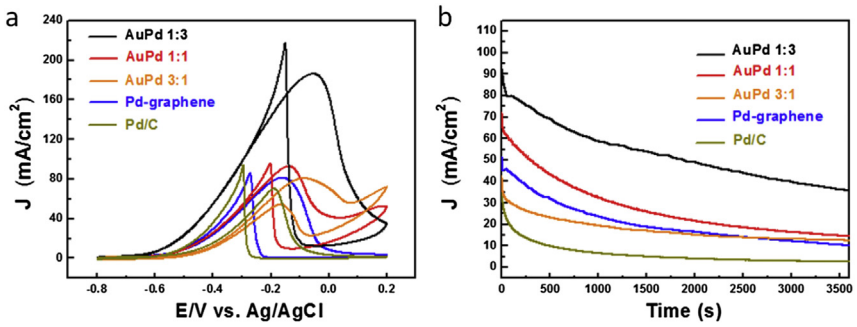

Fig. 6 – (a) Cyclic voltammograms of for ethanol electro-oxidation of graphene-supported AuPd alloy NPs with different Au-to-Pd ratios, where data of commercial Pd/C catalyst and graphene-supported Pd monometallic NPs are shown for reference. (b) Corresponding current density vs time of the catalysts shown in (a), carried out at −0.25 V in 1 M KOH + 1 M C_2H_5OH.

well, which can be ascribed to the size reduction of AuPd NPs. Upon increased addition of Pd, the diffraction patterns for AuPd (1:1) and AuPd (3:1) are similar to those of Pd monometallic NPs. Significantly, as demonstrated in Fig. 4, the Au (111) peak shifts toward the Pd (111) peak when decreasing the Au-to-Pd ratio, supporting the argument of the formation of AuPd alloy NPs [24,39–42].

The surface chemistry of the supported metal NPs is characterized by XPS, and the Au 4f and Pd 3d core level spectra are shown in Fig. 5. The two peaks in Fig. 5a can be assigned to the Au $4f_{5/2}$ and $4f_{7/2}$ states of zero-valent Au. The binding energies of Au $4f_{7/2}$ for Au-only, AuPd (3:1), AuPd (1:1) and AuPd (1:3) are 84.0, 84.0, 83.9 and 83.8 eV, respectively, which decrease with increasing the Pd content. The binding energy shift implies the charge transfer between Au and Pd. On the other hand, as demonstrated in Fig. 5b, the shoulder peak (~337.5 eV) at higher binding energy of Pd $3d_{5/2}$ is decreased upon increasing Au-to-Pd ratio. As the shoulder peak arises from oxidative Pd, the dilution of Pd by Au can suppress surface oxidation of Pd and improve its air stability [22,35,43]. The XPS results are in good agreement with the microscopic and crystalline characterization, indicating the occurrence of alloying in the supported AuPd NPs.

In order to study the synergistic effect in the AuPd alloy NPs, whose catalytic activity for ethanol electro-oxidation in an alkaline electrolyte is evaluated and compared with a commercial Pd/C catalyst. Fig. 6a shows the CV curves with two featured oxidation peaks during a round scan. The oxidation peak in the forward scan can be attributed to the oxidation of the chemisorbed species arising from ethanol adsorption, while the oxidation peak in backward scan can refer to the removal of the carbonaceous species which are not completely oxidized in forward scan. The derived specific activity for AuPd (1:3) is 186 mA/cm^2, which is much higher than 70 mA/cm^2 for commercial Pd/C and 81 mA/cm^{2}for the Pd monometallic counterpart. It is also higher than 90 mA/cm^{2}for AuPd (1:1) and 81 mA/cm^{2}for AuPd (3:1). In addition, the onset potential of AuPd (1:3) is about −0.68 V which is lower than that of commercial Pd/C. The results demonstrate the enhancement in catalytic activity for ethanol electro-oxidation upon alloying of Au and Pd with an appropriate Au-to-Pd ratio.

As shown in Fig. 6b, the operational stability of the catalysts is tested by the long-term CA measurements. The current decay for the AuPd alloy NPs is significantly slower than that for commercial Pd/C, indicating their better endurance in the ethanol electro-oxidation reaction. Furthermore, the residual current of AuPd (1:3) is larger than those of commercial Pd/C and the other compared catalysts, confirming the highest catalytic performance for AuPd (1:3).

It has been known that the addition of Au into Pd catalysis can enhance catalytic activity and selectivity as well as the resistance to poisoning, which also can summarize from CA and CV results in Fig. 6. Wang et al. propose a new method, relative reactivity retention (RRR) values, to quantitatively assess the anti-poisoning performance of anode catalysts via evaluating CA currents with reference to CV currents [32]. The RRR is defined as I_{CA}/I_{CV}, where the I_{CA} refers to the CA current at certain time point while I_{CV} refers to the corresponding CV current at −0.25 V obtained from the forward scan curves. Therefore, a higher RRR value for a catalyst means a higher anti-poisoning performance. From the Table 1 we can see that the RRR values of Pd-based NPs supported on graphene are all far larger than that of commercial catalysts, which is supported on active carbon (5.7% at 3500 s), indicating superior anti-poisoning effect of as-prepared catalysts supported on graphene than on active carbon. Meanwhile, compared with Pd-graphene (16.1% at 3500 s), all AuPd alloy NPs catalysts

Table 1 – A comparison in anti-poisoning performance of supported AuPd alloy NPs and Pd monometallic NPs based upon CA and CV results.

		500 s	1500 s	2500 s	3500 s
AuPd 1:3	I_{CA}/mAcm^{-2}	69.8	54.4	44.5	36.5
	RRR/%	57.5	44.8	36.7	30.1
AuPd 1:1	I_{CA}/mAcm^{-2}	43.4	25.8	18.7	14.8
	RRR/%	65.3	38.8	28.1	22.2
AuPd 3:1	I_{CA}/mAcm^{-2}	23.3	17.1	13.7	12.3
	RRR/%	50.2	36.8	29.5	26.5
Pd-G	I_{CA}/mAcm^{-2}	34.9	18.9	13.7	10.2
	RRR/%	50.1	29.7	21.5	16.1
Pd/C	I_{CA}/mAcm^{-2}	10.1	5.2	3.5	3.0
	RRR/%	19.2	9.9	6.7	5.7

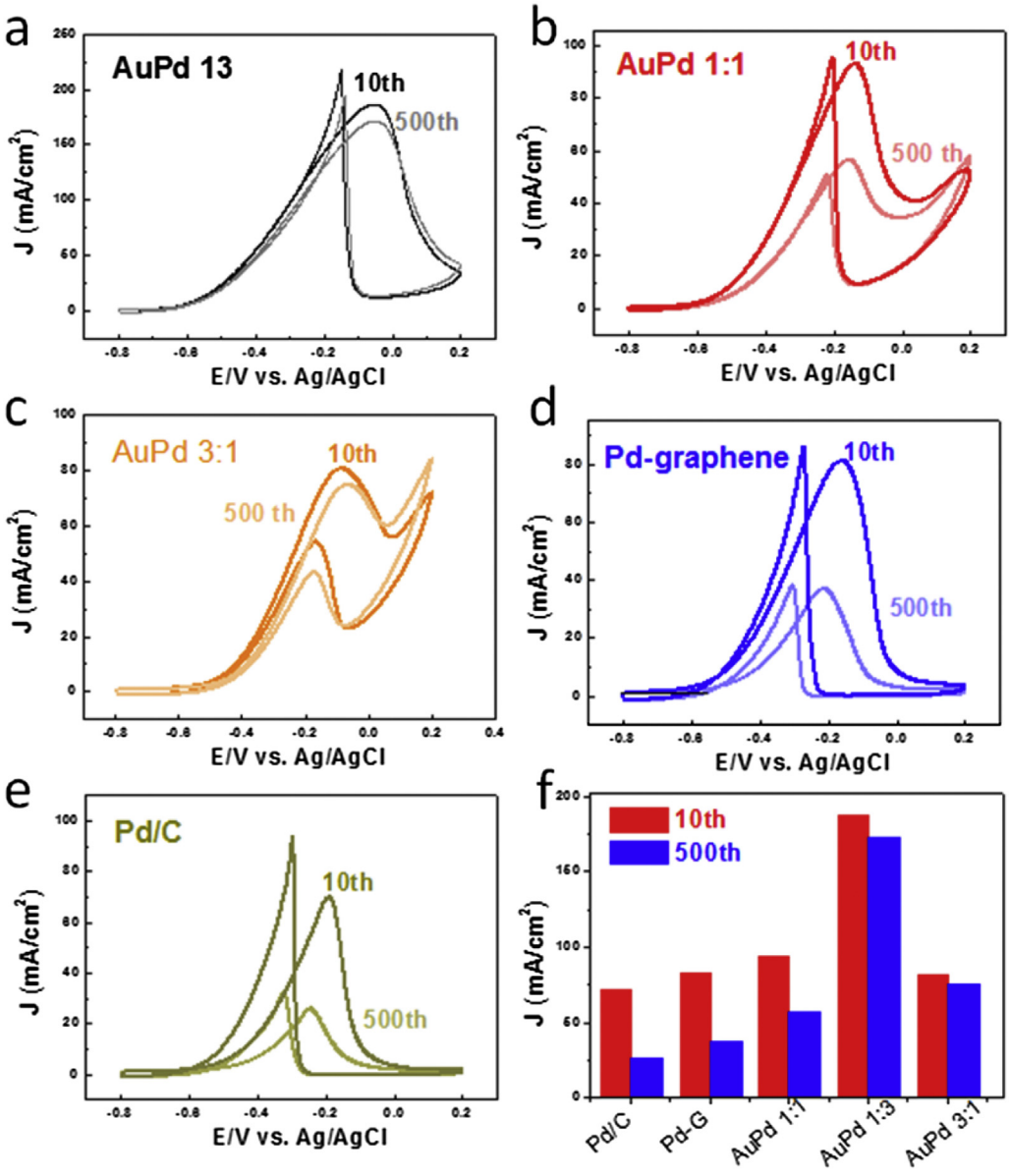

Fig. 7 – Cyclic voltammograms for ethanol electro-oxidation to evaluate the durability of (a) AuPd (1:3), (b) AuPd (1:1), (c) AuPd (3:1), (d) Pd-only and (e) commercial Pd/C catalysts; (f) A comparison of specific anodic current density between 10th and 500th cycles for the catalysts shown in (a)–(e), 1 M KOH + 1 M C_2H_5OH.

show higher RRR values, further confirming the higher anti-poisoning performance of alloy NPs than monometallic NPs because of the synergistic effect between Au and Pd components.

Fig. 7 shows a comparison of the initial catalytic behavior and that after repeated use. Using the anodic peak current density in forward scan after 10 CV cycles as the reference, the peak current density for AuPd (1:3) retains about 91% of activity after 500 CV cycles. This is much greater than 37% for commercial Pd/C and 46% for the Pd monometallic counterpart. Therefore, the AuPd alloy NPs show higher catalytic stability compared with their monometallic counterparts, which is critical to practical applications for DAFCs.

Conclusions

A straightforward approach, by the employment of an alloy target for the RTIL-assisted sputtering, has been developed to prepare the AuPd alloy NPs on graphene. The graphene-supported alloy NPs can act as a catalyst for ethanol electro-oxidation with both high catalytic activity and high stability, which are far superior to the performance of a commercial Pd/C catalyst. The synergistic effect between alloy components and the support effect will enhance the anti-poisoning performance of catalysts. The compositional ratio in the alloy NPs can be controlled simply by the selection of alloy targets, and the optimal Au-to-Pd ratio turns out to be 1:3 in the present

case. The current strategy opens a new opportunity to design and tailor the composition of alloy NPs for catalysis and energy applications.

Acknowledgments

This work was supported by the National Natural Science Foundation of China (Nos. 61274019, 11661131002), the Collaborative Innovation Center of Suzhou Nano Science & Technology, and the Priority Academic Program Development of Jiangsu Higher Education Institutions (PAPD).

REFERENCES

[1] Kamarudin MZF, Kamarudin SK, Masdar MS, Daud WRW. Review: direct ethanol fuel cells. Int J Hydrogen Energy 2013;38:9438–53.
[2] An L, Zhao TS. Performance of an alkaline-acid direct ethanol fuel cell. Int J Hydrogen Energy 2011;36:9994–9.
[3] Tiwari JN, Tiwari RN, Singh G, Kim KS. Recent progress in the development of anode and cathode catalysts for direct methanol fuel cells. Nano Energy 2013;2:553–78.
[4] Han LJ, Ju H, Xu YH. Ethanol electro-oxidation: cyclic voltammetry, electrochemical impedance spectroscopy and galvanostatic oscillation. Int J Hydrogen Energy 2012;37:15156–63.
[5] Hong W, Wang J, Wang E. Facile synthesis of highly active PdAu nanowire networks as self-supported electrocatalyst for ethanol electrooxidation. ACS Appl Mater Interface 2014;6:9481–7.
[6] Abdullah S, Kamarudin SK, Hasran UA, Masdar MS, Daud WRW. Modeling and simulation of a direct ethanol fuel cell: an overview. J Power Sources 2014;262:401–6.
[7] Ksar F, Surendran G, Ramos L, Keita B, Nadjo L, Prouzet E, et al. Palladium nanowires synthesized in hexagonal mesophases: application in ethanol electrooxidation. Chem Mater 2009;21:1612–7.
[8] Liu J, Ye J, Xu C, Jiang SP, Tong Y. Kinetics of ethanol electrooxidation at Pd electrodeposited on Ti. Electrochem Commum 2007;9:2334–9.
[9] Qiu JD, Wang GC, Liang RP, Xia XH, Yu HW. Controllable deposition of platinum nanoparticles on graphene as an electrocatalyst for direct methanol fuel cells. J Phys Chem C 2011;115:15639–45.
[10] Yoo E, Okata T, Akita T, Kohyama M, Nakamura J, Honma I. Enhanced electrocatalytic activity of Pt subnano clusters on graphene nanosheet surface. Nano Lett 2009;9:2255–9.
[11] Sun SH, Zhang GX, Gauquelin N, Chen N, Zhou JG, Yang SL, et al. Single-atom catalysis using Pt/graphene achieved through atomic layer deposition. Sci Rep 2013;3. http://dx.doi.org/10.1038/srep01775.
[12] Nassr ABAA, Sinev I, Pohl MM, Grünert W, Bron M. Rapid microwave-assisted polyol reduction for the preparation of highly active PtNi/CNT electrocatalysts for methanol oxidation. ACS Catal 2014;4:2449–62.
[13] Cai JD, Huang YY, Guo YL. Facile synthesis of $PdSb_x$/C nanocatalysts with high performance for ethanol electro-oxidation in alkaline medium. Int J Hydrogen Energy 2014;39:18256–63.
[14] Mukherjee P, Roy PS, Bhattacharya SK. Improved carbonate formation from ethanol oxidation on nickel supported Pt-Rh electrode in alkaline medium at room temperature. Int J Hydrogen Energy 2015;40:13357–67.
[15] Hu CG, Cheng HH, Zhao Y, Hu Y, Liu Y, Dai LM, et al. Newly-designed complex ternary Pt/PdCu nanoboxes anchored on three-dimensional graphene framework for highly efficient ethanol oxidation. Adv Mater 2012;24:5493–8.
[16] Hu CY, Wang X. Highly dispersed palladium nanoparticles on commercial carbon black with significantly high electro-catalytic activity for methanol and ethanol oxidation. Int J Hydrogen Energy 2015;40:12382–91.
[17] Shen SY, Zhao TS, Xu JB, Li YS. Synthesis of PdNi catalysts for the oxidation of ethanol in alkaline direct ethanol fuel cells. J Power Sources 2010;195:1001–6.
[18] Wang D, Xin HL, Yu Y, Wang H, Rus E, Muller DA, et al. Pt-decorated PdCo@ Pd/C core–shell nanoparticles with enhanced stability and electrocatalytic activity for the oxygen reduction reaction. J Am Chem Soc 2010;132:17664–6.
[19] Shao M, Sasaki K, Marinkovic NS, Zhang L, Adzic RR. Synthesis and characterization of platinum monolayer oxygen–reduction electrocatalysts with Co–Pd core–shell nanoparticle supports. Electrochem Commum 2007;9:2848–53.
[20] Venezia AM, Liotta LF, Deganello G, Schay Z, Guczi L. Characterization of pumice-supported Ag–Pd and Cu–Pd bimetallic catalysts by X-ray photoelectron spectroscopy and X-ray diffraction. J Catal 1999;182:449–55.
[21] Liu AH, Geng HR, Xu CX,Qiu HJ. A three-dimensional hierarchical nanoporous PdCu alloy for enhanced electrocatalysis and biosensing. Anal Chim Acta 2011;703:172–8.
[22] Chen LY, Chen N, Hou Y, Wang ZC, Lv SH, Fujita T, et al. Geometrically controlled nanoporous PdAu bimetallic catalysts with tunable Pd/Au ratio for direct ethanol fuel cells. ACS Catal 2013;3:1220–30.
[23] Qiu X, Dai Y, Tang Y, Lu T, Wei S, Chen Y. One-pot synthesis of gold–palladium@ palladium core–shell nanoflowers as efficient electrocatalyst for ethanol electrooxidation. J Power Sources 2015;278:430–5.
[24] Lee YW, Kim M, Kim Y, Kang SW, Lee JH, Han SW. Synthesis and electrocatalytic activity of Au–Pd alloy nanodendrites for ethanol oxidation. J Phys Chem C 2010;114:7689–93.
[25] Gao F, Goodman DW. Pd–Au bimetallic catalysts: understanding alloy effects from planar models and (supported) nanoparticles. Chem Soc Rev 2012;41:8009–20.
[26] Gao F, Goodman DW. Model catalysts: simulating the complexities of heterogeneous catalysts. Annu Rev Phys Chem 2012;63:265–86.
[27] Yi CW, Luo K, Wei T, Goodman DW. The composition and structure of Pd-Au surfaces. J Phys Chem B 2005;109:18535–40.
[28] Geim AK. Graphene: status and prospects. Science 2009;324:1530–4.
[29] Pumera M, Wong CHA. Graphane and hydrogenated graphene. Chem Soc Rev 2013;42:5987–95.
[30] Stankovich S, Dikin DA, Dommett GH, Kohlhaas KM, Zimney EJ, Stach EA, et al. Graphene-based composite materials. Nature 2006;442:282–6.
[31] Marquardt D, Vollmer C, Thomann R, Steurer P, Mülhaupt R, Redel E, et al. The use of microwave irradiation for the easy synthesis of graphene-supported transition metal nanoparticles in ionic liquids. Carbon 2011;49:1326–32.
[32] Wang JS, Liu CH, Banis MN, Cheng NC, Riese A, Wang SD, et al. Superior anti-poisoning performance of graphenes versus carbon nanotubes as Pt catalysts supports for formate oxidation. Int J Hydrogen Energy 2015;41:936–43.
[33] Liu CH, Mao BH, Gao J, Zhang S, Gao X, Liu Z, et al. Size-controllable self-assembly of metal nanoparticles on carbon nanostructures in room-temperature ionic liquids by simple sputtering deposition. Carbon 2012;50:3008–14.

[34] Liu CH, Chen XQ, Hu YF, Sham TK, Sun QJ, Chang JB, et al. One-pot environmentally friendly approach toward highly catalytically active bimetal-nanoparticle-graphene hybrids. ACS Appl Mater Interfaces 2013;5:5072–9.
[35] Liu CH, Liu RH, Sun QJ, Chang JB, Gao X, Liu Y, et al. Controlled synthesis and synergistic effects of graphene-supported PdAu bimetallic nanoparticles with tunable catalytic properties. Nanoscale 2015;7:6356–62.
[36] Chang JB, Liu CH, Liu J, Zhou YY, Gao X, Wang SD. Green-chemistry compatible approach to TiO_2-supported PdAu bimetallic nanoparticles for solvent-free 1-phenylethanol oxidation under mild conditions. Nano-Micro Lett 2015;7:307–15.
[37] Dupont J, Scholten JD. On the structural and surface properties of transition-metal nanoparticles in ionic liquids. Chem Soc Rev 2010;39:1780–804.
[38] Zhang Y, Zhang N, Tang ZR, Xu YJ. Graphene oxide as a surfactant and support for in-situ synthesis of Au–Pd nanoalloys with improved visible light photocatalytic activity. J Phys Chem C 2014;118:5299–308.
[39] Wang RY, Wu ZW, Chen CM, Qin ZF, Zhu HQ, Wang GF, et al. Graphene-supported Au–Pd bimetallic nanoparticles with excellent catalytic performance in selective oxidation of methanol to methyl formate. ChemCommun 2013;49:8250–2.
[40] Rao CV, Cabrera CR, Ishikawa Y. Graphene-supported Pt–Au alloy nanoparticles: a highly efficient anode for direct formic acid fuel cells. J Phys Chem C 2011;115:21963–70.
[41] Teng XW, Wang Q, Liu P, Han WQ, Frenkel AI, Wen W, et al. Formation of Pd/Au nanostructures from Pd nanowires via galvanic replacement reaction. J Am Chem Soc 2008;130:1093–101.
[42] Liu F, Wechsler D, Zhang P. Alloy-structure-dependent electronic behavior and surface properties of Au–Pd nanoparticles. Chem Phys Lett 2008;461:254–9.
[43] Torimoto T, Okazaki K, Kiyama T, Hirahara K, Tanaka N, Kuwabata S. Sputter deposition onto ionic liquids: simple and clean synthesis of highly dispersed ultrafine metal nanoparticles. Appl Phys Lett 2006;89:243117.